Ferromagnetism, Jahn-Teller effect, and orbital order in the two-dimensional monolayer perovskite math xmlns="http://www.w3.org/1998/Math/MathML">mrow>msub>mi>Rb/mi>mn>2/mn>/msub>msub>mi>CuCl/mi>mn>4/mn>/msub>/mrow>/math>

Chao Liu, Guodong Zhao, Tao Hu, Yangyang Chen, Shixun Cao, L. Bellaiche, and Wei Ren

Phys. Rev. B **104**, L241105 — Published 16 December 2021

DOI: 10.1103/PhysRevB.104.L241105

Ferromagnetism, Jahn-Teller effect, and orbital order in 2D monolayer perovskite Rb_2CuCl_4

Chao Liu[1,2], Guodong Zhao[1], Tao Hu[1]*, Yangyang Chen[1]*, Shixun Cao[1], L. Bellaiche[2], and Wei Ren[1]*

1 Physics Department, State Key Laboratory of Advanced Special Steel, Shanghai Key Laboratory of High Temperature Superconductors, International Centre of Quantum and Molecular Structures, Shanghai University, Shanghai 200444, China

2 Physics Department and Institute for Nanoscience and Engineering, University of Arkansas, Fayetteville, Arkansas 72701, USA

* taohu@shu.edu.cn; phycyy@shu.edu.cn; renwei@shu.edu.cn

Abstract

Two-dimensional (2D) ferromagnetic (FM) semiconductors have attracted increasing interest for advanced spintronics. Here, we report that monolayer perovskite Rb_2CuCl_4 (RCC) exhibits intrinsic 2D FM semiconductor feature, emergent Jahn-Teller (JT) effect and related orbital order (OO) with the diversity and tunability of physical behaviors. First-principle calculations and Monte Carlo (MC) simulations reveal the crucial changes of OO type, related mechanism of ferromagnetism, and electronic structure during the transition of JT distortion. Finally, we examine the significant tunable effect of biaxial strain on electronic and magnetic properties. Our comprehensive work on magnetism, structural distortion, and electronic properties of monolayer RCC provide a guideline for studying physical phenomena of $3d^9$ Cu(II) in 2D halide perovskites.

Introduction

Two-dimensional (2D) ferromagnetic (FM) semiconductors have been recognized as a cornerstone of spintronic applications, such as data storage, capacitors, and logical devices [1,2]. Recently, many relevant systems have been synthesized and studied both in theory and experiment. Most notably, the successful preparation of CrI_3 [3] and $Cr_2Ge_2Te_6$ [4] proves that 2D long-range magnetic orders could exist, enhanced by magnetic anisotropy. A number of investigations on layered magnetic materials followed, including VI_3 [5,6], $CrBr_3$ [7], and $CrCl_3$ [8,9], which have a similar hexagonal structure [10]. Meanwhile, more 2D FM semiconductors have attracted tremendous research interest in calculations, such as the 2H-phase VS_2 that is an easy-plane FM semiconductor [11,12], $CrWGe_2Te_6$ and $Cr_2Ge_2Se_6$ monolayers that are predicted to be room-temperature FM semiconductors [13,14]; and a number of 2D semiconductors that could exhibit record-higher critical temperature (T_C) [15,16].

Perovskite materials which contain transition metal elements are important to the study of intrinsic magnetism, but there is still limited progress on 2D Ruddlesden-Popper (RP) perovskites with ferromagnetism. Recent, synthesis of single-layer structure demonstrated that atomically ultrathin perovskite can exist [17,18]. Besides oxides, a class of layered perovskite halides are excellent candidates for the exploration of 2D ferromagnetism, e.g., the RP perovskites K_2CuF_4, Cs_2AgF_4, and Rb_2CrCl_4 with

the general formula of A_2BX_4. They exhibit FM or interlayer antiferromagnetic (AFM) configurations in experiments [19-21], and the structure and magnetism of layered perovskites in 2D form are also under investigation [22-26]. Moreover, Jahn-Teller (JT) effect and orbital order (OO) [27-30] in perovskite could further increase the tunability of physical behaviors, e.g., the elimination of electronic degeneracy, opening of band gap and variation of magnetic properties.

In this work, we study the layered halide perovskite Rb_2CuCl_4 (RCC) to report its structural and magnetic properties in two dimensions. Particularly, we focus on ferromagnetism, JT effect, OO, and their interactions. The structural ground state is determined by analyzing the phonon vibrational mode and energy barrier. By means of meticulous magnetic and electronic calculations, as well as Monte Carlo (MC) simulations, we demonstrate that monolayer RCC shows excellent ferromagnetic semiconductor characteristics with in-plane magnetic moments and T_C close to that of bulk. We characterize the significant relevance of JT distortion, electronic structure, OO, magnetic behavior, and semiconductor-metal transition during the transition from a tetragonal to an orthorhombic phase. Additional calculations also show that biaxial strain directly dominates JT distortion and further affects the magnetic behavior, such as the ground-state magnetic configuration and magnetic anisotropy.

Results and Discussion

The RP perovskite family has been a subject of many investigations that focuses on clarifying the role of dimensionality on electronic and magnetic properties. RCC is the first (n = 1) member of the RP series $Rb_{n+1}Cu_nX_{3n+1}$, n = 1, 2, ..., ∞. The magnetic layered RP perovskites usually exhibit different ground state structures at cryogenic temperatures, distinguished by the presence or absence of JT distortion. For example, K_2NiF_4 is AFM with a tetragonal phase (space group Fm-3m) [31] and Cs_2AgF_4 is FM with an orthorhombic phase (space group Cmcm) [32]. In contrast, bulk RCC shows an orthorhombic ground state with a layered AFM configuration in experiment, which makes it a good candidate for studying 2D ferromagnetism [33]. Figure 1(a) shows the top and side views of monolayer RCC. The octahedra formed by blue copper (Cu) and surrounding green chlorine (Cl) atoms are connected in a corner-sharing manner and are enveloped in a square lattice formed by purple Rubidium (Rb) atoms. The length difference between the *a* and *b* axes is less than 0.01 □, thus we set *a* = *b* for convenience, which should not affect the results of crystal and electronic structures calculation. Then, we find the optimized Cu-Cl bond lengths, l_1 = 2.27 □, and l_2 = 2.72 □ as shown in Fig. 1(b), which indicate that single-layer RCC keeps the characteristics of JT distortions. Besides, we obtain its cleavage energy for the optimized structure by taking into account the van der Waals correction. In Fig. 1(c), the calculated cleavage energy 0.33 J/m^2 is much lower than that of K_2CuF_4 [22] and K_2CoF_4 [26], and quite close to that of graphite [34], confirming the possibility of creating RCC monolayer via mechanical exfoliation.

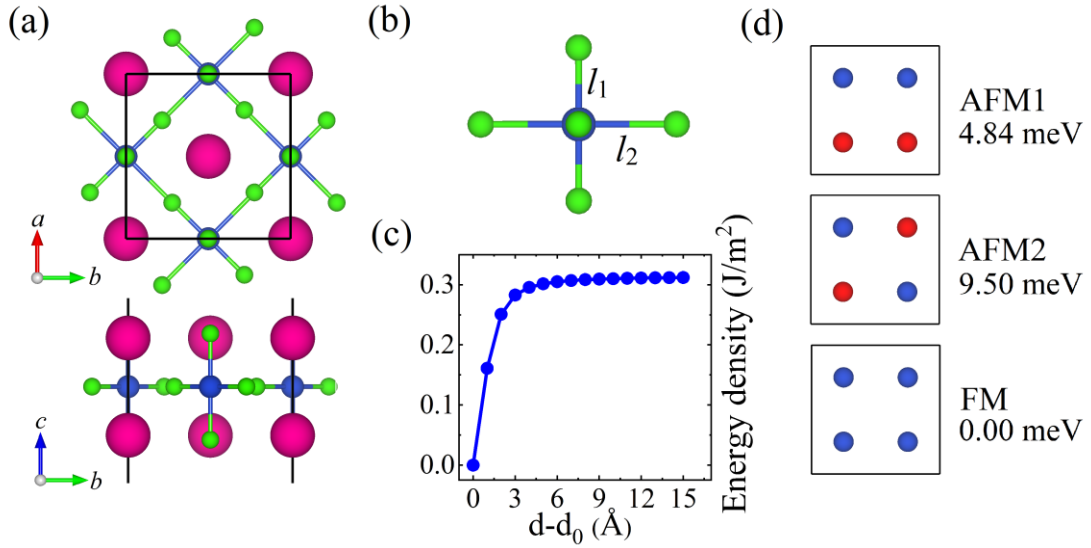

Figure 1. (a) The top and side views of monolayer Rb_2CuCl_4 (RCC). The purple, blue, and green balls represent Rb, Cu, and Cl atoms respectively. (b) Individual Cu-Cl octahedron with JT effect, l_1 and l_2 correspond to the short and long Cu-Cl bonds. (c) The calculated cleavage energy of RCC, d and d_0 represent the interlayer separation and its value in the equilibrium configuration. (d) Sketches of the different spin configurations, with only the transition-metal ions shown. The blue and red dots represent opposite spin directions.

To describe the 2D magnetic configurations, we constructed $\sqrt{2}\times\sqrt{2}$ supercells with four Cu atoms. Here, we consider three possible collinear magnetic orderings, namely AFM1, AFM2, and FM configurations, as schematically shown in Fig. 1(d). From their relative energies, we find that the most stable one is the FM, with the AFM1 and AFM2 configurations are 4.84 meV and 9.50 meV, which are both higher in energy than the FM configuration. The net magnetic moment is found to be 1 μ_B/formula unit, indicating a 2D spin = 1/2 ferromagnet. In addition, we include different Coulomb Repulsion U values from 0 to 8 eV for monolayer RCC, to verify that the FM ground state is maintained by considering different electronic correlation strengths, as shown in Fig. S1 in the Supplemental Material [35].

As RCC-related halide perovskites usually display tetragonal or orthorhombic structure, it is necessary to study whether this original structural feature can be maintained in two dimensions. Thus, we performed phonon dispersion calculation for both the tetragonal phase without JT distortion and orthorhombic phase with JT distortion. For the tetragonal phase, an acoustic branch with imaginary frequency at the M point appears, as shown in Fig. S2(a) in [35]. We find that the length variation in *ab* plane of Cu-Cl bond causes the atomic displacements corresponding to the imaginary acoustic mode, which is also consistent with the JT distortion in the bulk. As for the orthorhombic phase, it turns out that there is no imaginary frequency in the whole Brillouin zone. These results thus show that RCC with a orthorhombic structure is an appropriate candidate to exhibit JT distortions in two dimensions.

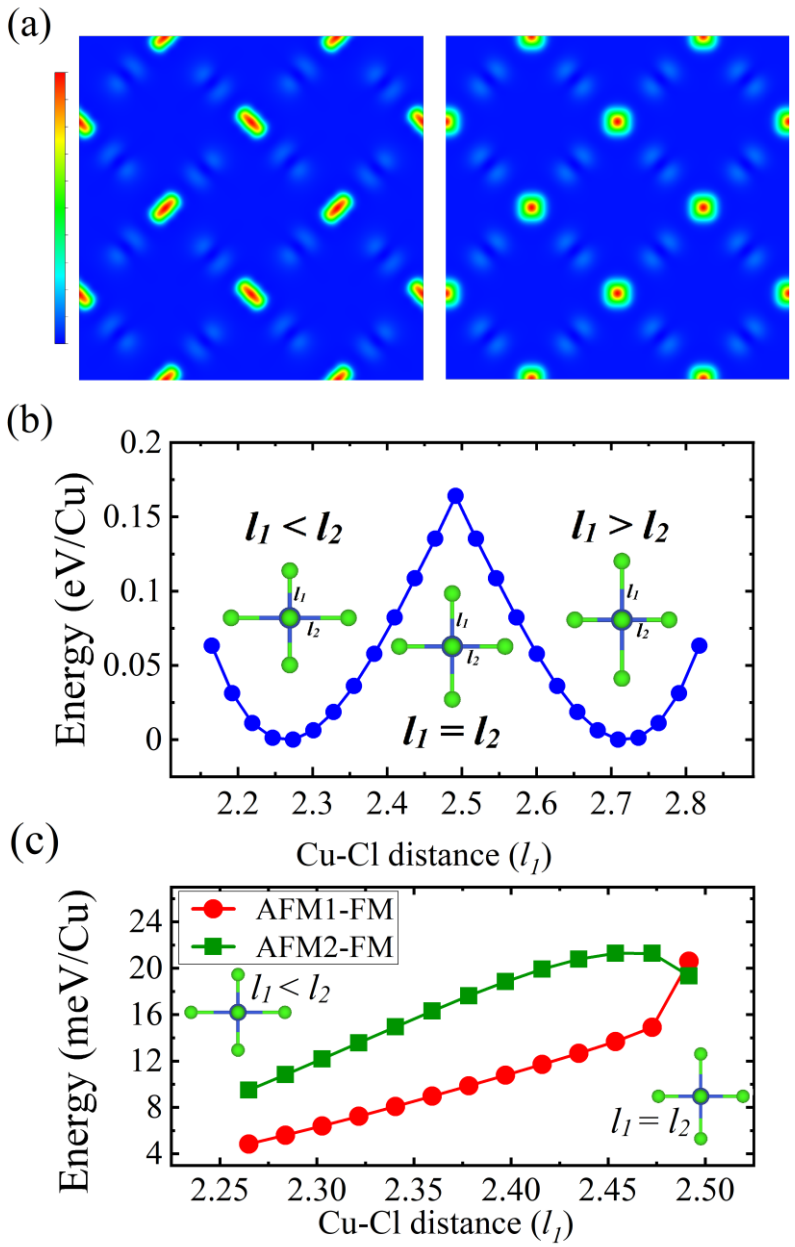

Figure 2. (a) Spin densities of the orthorhombic (left) and tetragonal (right) phases on the (*0 0 1*) plane. (b) Potential energy barrier of JT distortion (FM state) with different Cu-Cl bond lengths. The l_1 and l_2 of ground states are 2.26 and 2.72 Å, respectively. (c) The energy difference between AFM and FM magnetic states during the transition of JT distortions.

It is known that for layered perovskites similar to RCC such as Cs_2AgF_4 and K_2CuF_4, JT distortion and OO play an important role to stabilize intralayer FM configuration [20,36-38]. We present the staggered OO of orthorhombic phase with $d_{x^2-z^2}$ and $d_{y^2-z^2}$ orbitals in the monolayer RCC as the evidence for the OO-induced FM ground state, as shown in the left of Fig. 2(a). Clearly, the staggered OO is intimately linked to JT distortion, which becomes regular OO when the structure is

transformed to a tetragonal phase, with the result of an intralayer AFM exchange interaction. This phenomena is different from $KCuF_3$, in which "pre-existing" electronically driven orbital polarization is observed even in the undistorted phase [39]. The potential barrier of JT effect is also calculated, as shown in Fig. 2(b). The horizontal axis shows the Cu-Cl bond length (l_1), whose increase is accompanied by the decrease of the l_2 bond length and vice versa. The JT barrier is found to be 0.16 eV. During the transition from orthorhombic to tetragonal phase, magnetic interaction of monolayer RCC also changes, as shown in Fig. 2(c). The red sphere and the green square data indicate the energy difference between the two AFM configurations and the FM configuration, respectively. When the structure approaches the case of $l_1 = l_2$, it is clear that both energy differences gradually increase, indicating an enhancement of FM interaction. Unusually, we find in Fig. 2(c) that the distinct variation appears when the OO changes from staggered order to regular order. This phenomenon reveals that the change of OO may have an important effect on the magnetic interaction. However, the FM ground state of monolayer RCC is unchanged for the regular OO situation, and the electronic structure of the tetragonal phase becomes half-metallic in nature, with the spin-down band passing through the Fermi level, as shown in Fig. S3 in [35]. These are similar to the electronic and magnetic characteristics of tetragonal bulk Cs_2AgF_4 with itinerant magnetism [36,40], suggesting that the FM ground state of tetragonal and orthorhombic phases is dominated by different mechanisms. Therefore, we conclude that monolayer RCC has stable ferromagnetism, which is unaffected by JT distortions and OO variations. It is worth mentioning that our calculated OO results of monolayer RCC are identical to the reported RCC bulk in experiments [33]. The above calculation results indicate the significant concerning on the study of physical properties from the tetragonal phase to orthorhombic phase of monolayer RCC, involving point groups, electronic structures, orbital order, magnetic ground states, semiconductor-metal transitions, and their interaction.

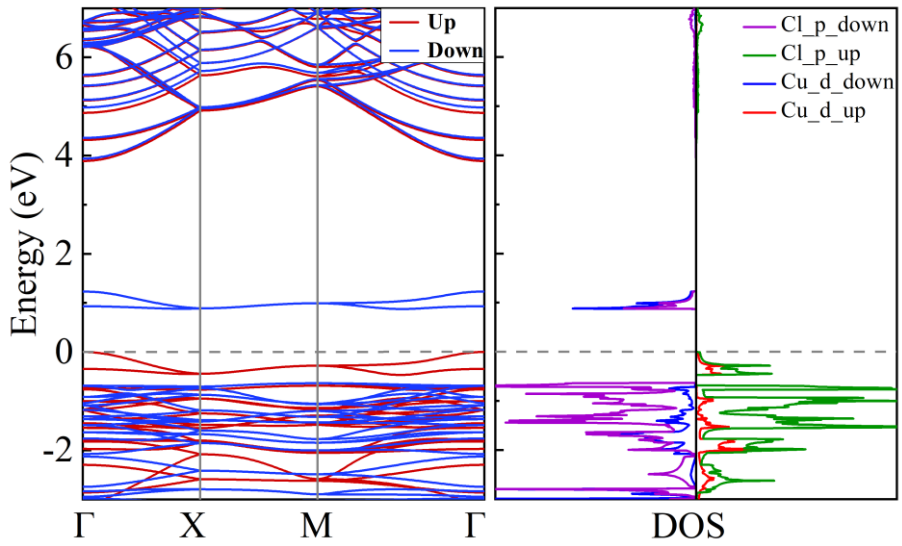

Figure 3. The calculated band structure and corresponding DOS of the RCC orthorhombic phase. (a) and (b)

After the study of the JT effect and OO of RCC monolayer, we now focus on the electronic properties of orthorhombic and tetragonal phases. Figure 3 shows the spin-dependent band structure with GGA + U and the corresponding density of states (DOS) of monolayer RCC. It can be seen that the ground-state orthorhombic phase shows semiconductor property with a band gap of 0.87 eV. Its spin-up and spin-down band gaps are 3.89 eV and 1.51 eV, respectively. However, the tetragonal phase of monolayer RCC exhibits half-metallic characteristic with spin-down band passing through the Fermi level. For valence and conduction bands around the Fermi level, we find that the *p*-orbital of Cl has a significant contribution to both the valence and conduction bands, which indicates that *d*-orbital of Cu and *p*-orbital of Cl experience some hybridization. The DOS below the Fermi level is mainly contributed by *p*-orbital of Cl ions, and the spin-down conduction bands are mainly contributed by *d*-orbital of Cu ions. The *p*-orbital of Cl has a considerable effect for spin-up valence and spin-down conduction bands resulting from *d*-orbital of Cu ions. This is also confirmed by the presence of local magnetic moment on each ion. We note that almost all of spin-polarized electrons in the RCC monolayer are located around the *d*-orbital of copper and *p*-orbital of chloride ions, resulting in local magnetic moment of about 0.55 μ_B/Cu and ~0.1 μ_B/Cl, whereas magnetic moments show zero on rubidium and other orbitals. This is also confirmed by observable contribution of the p orbital of Cl to the spin density in Fig. 2(a).

Magnetic anisotropy is crucial for establishing long-range 2D ferromagnetism, which determines the easy magnetization axis, and can be evaluated by total energy as a function of magnetization direction with spin-orbital coupling. Before analyzing the calculated results, let us also recall that synthesized bulk RCC displays interlayered AFM configuration with in-plane magnetic moment and a weak *ab* plane anisotropy; experiments also reported a Néel temperature of 20 K, above which it becomes paramagnetic in nature [41]. Therefore, we calculated the angular dependent magnetic anisotropic energy (MAE) by scanning the *ab* and *ac* planes in monolayer RCC, and our results indicate that monolayer is in-plane FM with *ac*-plane MAE of 35 μeV/Cu in Fig. S4(a) in the Supplemental Material [35]. The magnetic behavior and MAE of RCC monolayer is thus close to that of $CrCl_3$ monolayer [42,43]. Moreover, we found that the anisotropy of in-plane FM is quite small and significantly affected by the lattice as shown in Fig. S4(b) in [35]. The MAE of *ab* plane increases with the increase of the *ab* lattice difference, that is the difference between the *a*-axis and *b*-axis lattice constants, following a linear trend, indicating that the weak in-plane anisotropy is present and is thus not a numerical error. That is, under uniaxial strain the monolayer RCC may become an in-plane easy-axis ferromagnet, and the magnetic easy axis is along the shorter *a*-axis. It is worth mentioning that the *ab* lattice difference is as small as ~0.01 □ in the situation of fully optimized structure, and the value is close to 0.01 □ of bulk in experiment [33]. The easy-plane ferromagnetism suggests its FM direction can be easily controlled by an applied magnetic field, and the displayed in-plane isotropy with a strict square lattice ($a = b$) allows the study of the magnetic phase transition and related phenomena [8].

In order to understand the temperature effects on magnetism, we further perform

MC simulations on the basis of the XY model (suitable for describing easy-plane FM) to examine the critical temperature. Here, the spin Hamiltonian is expressed as:

$$\mathbf{H} = -2\mathrm{J}_1 \sum_{\langle ij \rangle} \boldsymbol{S}_i \cdot \boldsymbol{S}_j - 2\mathrm{J}_2 \sum_{\langle\langle ij \rangle\rangle} \boldsymbol{S}_i \cdot \boldsymbol{S}_j \quad (1)$$

where $\langle ij \rangle$ and $\langle\langle ij \rangle\rangle$ denotes the first and second nearest neighbor spins, and J_1, J_2 correspond to exchange coupling constants between the first and second nearest neighbor spins, respectively. The J_1, J_2 values are found to be 4.750 and 0.045 meV respectively. These parameters suggest that both the first and second nearest neighbor exchange interactions are FM, and almost all FM exchange is the contribution of the nearest neighbor interaction. Then, using these J values, we calculated the critical temperature T_C by performing MC simulation on the 2D supercell. The 20 × 20 square lattice with periodic conditions is set up, and the MC simulations run for 10^6 steps of equilibrium and 10^6 steps for statistics at each temperature point. The simulated T_C of monolayer RCC is found to be ~29 K, slightly higher than the value from experiment [33]. We also performed the MC simulation based on Heisenberg model considering the MAE, and obtained a magnetic transition temperature of 20 K, which is close to the transition temperature of bulk. The MC results of transition temperature for XY and Heisenberg models are illustrated in Fig. S5 in the Supplemental Material [35].

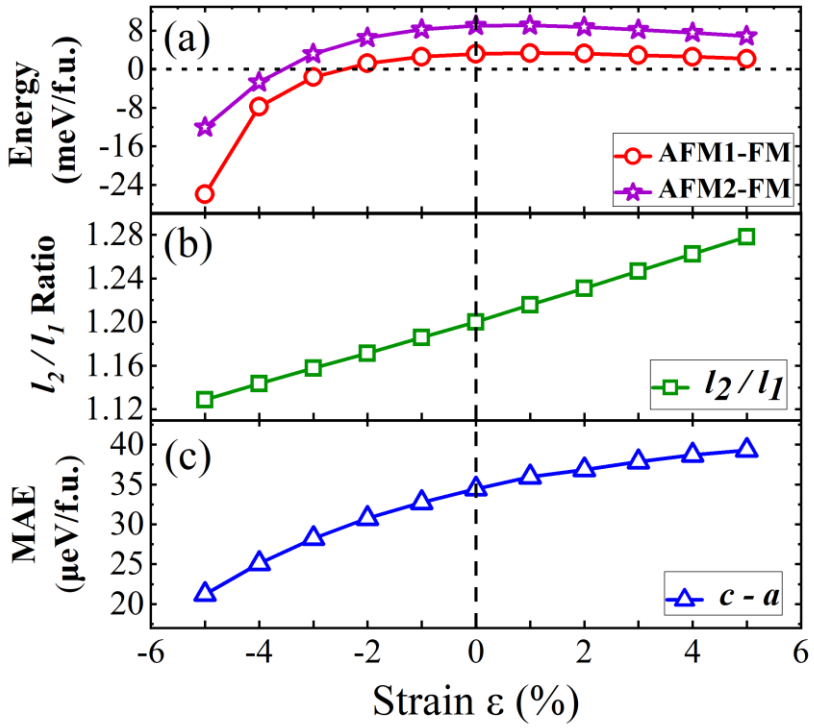

Figure 4. Effects of lattice strain on the (a) magnetic ground state, (b) Cu-Cl bond length ratio (l_2/l_1) of JT effect, and (c) MAE of RCC monolayer.

In addition, the effects of lattice strains on magnetic configurations and electronic structures are useful for applications in flexible devices [44,45]. In order to investigate such effects, we use the lattice ratio $\varepsilon = (a - a_0)/a_0$ to represent the value of biaxial strain,

for example, ε = 1% means the lattice constant is 1% larger than the strain-free condition. A negative valued ε is for compression while a positive valued ε represents tension. The energy and structural changes of RCC monolayer as functions of strain are displayed in Fig. 4. The purple stars and red circles in Fig. 4(a) are the energy differences between FM and two AFM magnetic configurations (AFM1-FM and AFM2-FM), respectively. We employ the Cu-Cl bond length ratio (l_2/l_1) to characterize the degree of JT effect and the green squares show its variation trend versus strain in Fig. 4(b), and no other structural distortion is caused by strain. The MAE represented by the blue triangles as a function of strain is shown in Fig. 4(c). We note that the system can maintain its in-plane FM ground state under strain of ε = 5% to −2%, below which is shown an AFM ground state. The phenomenon of pressure-induced AFM has also been reported in other perovskites and 2D crystals [46-48]. It is notable that the effect of strain may cause the RCC monolayer to exhibit an antiferromagnetic ground state while maintaining JT distortion. The result of MAE changes indicates that the magnetic moment direction of the RCC monolayer always prefers to lie in the *ab* plane, and the energy difference (between *c*-axis and *a*-axis FM) is positively correlated with strain ε. Interestingly, we find that the strain exhibits a significant regulating control on the JT distortion. As the lattice constant decreases, the ratio of l_2/l_1 (ranging from 1.28 to 1.13) shows a perfect linear relationship. We performed further calculations with regard to the total suppression of the JT effect, and found that the ratio is unity until ε = −8%. Therefore, the lattice strain is an effective way to manipulate JT effect and even eliminate it completely. The related works of pressure induced JT distortion reduction of bulk RCC have also been reported [49,50], which are in good agreement with our findings in this work.

Conclusion

In summary, we study from first-principles the magnetism, JT effect, and related OO properties of monolayer perovskite Rb_2CuCl_4. The cleavage energy and phonon spectrum prove its stability of the orthorhombic phase (with JT distortion) in two dimensions. We confirm its ferromagnetic ground state with magnetic moment of 1 μ_B/Cu by comparing the energy among different magnetic configurations. The obtained electronic structure indicates the interesting semiconductor characteristics with spin-up band gap of 3.89 eV and spin-down band gap of 1.51 eV, respectively. We also calculate the spin density of monolayer RCC to verify that the ferromagnetism is generated by intralayer staggered OO. Further, the investigations of JT barrier and corresponding changes in magnetism and OO suggest the appearance of regular OO in the tetragonal phase (without JT distortion), as well as the transformation from FM semiconducting to half-metallic feature. We find that the monolayer RCC is in-plane FM with a small MAE, thus the weak in-plane magnetic anisotropy behavior can be described by the XY model. MC simulation suggests the stable ferromagnetic ground state below 29 K. Finally, we investigate the strain effect on magnetism and distortion, revealing the robust ferromagnetism when ε > −3%, and the feasible control of JT distortion by lattice strain. These findings expand our understanding of 2D FM perovskites and their potential for spintronic applications.

Acknowledgments

This work was supported by the National Natural Science Foundation of China (51861145315, 11929401, 12074241), the Independent Research and Development Project of State Key Laboratory of Advanced Special Steel, Shanghai Key Laboratory of Advanced Ferrometallurgy, Shanghai University (SKLASS 2020-Z07), the Science and Technology Commission of Shanghai Municipality (19DZ2270200, 19010500500, 20501130600), and High Performance Computing Center, Shanghai University. L.B. thanks the DARPA Grant No. HR0011727183-D18AP00010 (TEE Program) and the Vannevar Bush Faculty Fellowship (VBFF) Grant No. N00014-20-1-2834 from the Department of Defense.

Reference

[1] K. S. Burch, D. Mandrus and J.-G. Park, Nature **563**, 47 (2018).
[2] K. S. Novoselov, D. Jiang, F. Schedin, T. Booth, V. Khotkevich, S. Morozov and A. K. Geim, Proceedings of the National Academy of Sciences **102**, 10451 (2005).
[3] B. Huang, G. Clark, E. Navarro-Moratalla, D. R. Klein, R. Cheng, K. L. Seyler, D. Zhong, E. Schmidgall, M. A. McGuire and D. H. Cobden, Nature **546**, 270 (2017).
[4] C. Gong, L. Li, Z. L. Li, H. W. Ji, A. Stern, Y. Xia, T. Cao, W. Bao, C. Z. Wang, Y. A. Wang, Z. Q. Qiu, R. J. Cava, S. G. Louie, J. Xia and X. Zhang, Nature **546**, 265 (2017).
[5] T. Kong, K. Stolze, E. I. Timmons, J. Tao, D. R. Ni, S. Guo, Z. Yang, R. Prozorov and R. J. Cava, Advanced Materials **31** (2019).
[6] G.-D. Zhao, X. Liu, T. Hu, F. Jia, Y. Cui, W. Wu, M.-H. Whangbo and W. Ren, Phys. Rev. B **103**, 014438 (2021).
[7] Z. W. Zhang, J. Z. Shang, C. Y. Jiang, A. Rasmita, W. B. Gao and T. Yu, Nano Letters **19**, 3138 (2019).
[8] X. Cai, T. Song, N. P. Wilson, G. Clark, M. He, X. Zhang, T. Taniguchi, K. Watanabe, W. Yao and D. Xiao, Nano letters **19**, 3993 (2019).
[9] H. H. Kim, B. Yang, S. Li, S. Jiang, C. Jin, Z. Tao, G. Nichols, F. Sfigakis, S. Zhong and C. Li, Proceedings of the National Academy of Sciences **116**, 11131 (2019).
[10] K. Wang, T. Hu, F. Jia, G. Zhao, Y. Liu, I. V. Solovyev, A. P. Pyatakov, A. K. Zvezdin and W. Ren, Applied Physics Letters **114**, 092405 (2019).
[11] X. Liu, A. P. Pyatakov and W. Ren, Phys. Rev. Lett. **125**, 247601 (2020).
[12] H. L. Zhuang and R. G. Hennig, Physical Review B **93**, 054429 (2016).
[13] C. Huang, J. Feng, F. Wu, D. Ahmed, B. Huang, H. Xiang, K. Deng and E. Kan, Journal of the American Chemical Society **140**, 11519 (2018).
[14] X.-J. Dong, J.-Y. You, B. Gu and G. Su, Physical Review Applied **12**, 014020 (2019).
[15] N. Miao, B. Xu, L. Zhu, J. Zhou and Z. Sun, Journal of the American Chemical Society **140**, 2417 (2018).
[16] A.-N. Ma, P.-J. Wang and C.-W. Zhang, Nanoscale **12**, 5464 (2020).
[17] G. Dong, S. Li, M. Yao, Z. Zhou, Y.-Q. Zhang, X. Han, Z. Luo, J. Yao, B. Peng and Z. Hu, Science **366**, 475 (2019).
[18] D. Ji, S. Cai, T. R. Paudel, H. Sun, C. Zhang, L. Han, Y. Wei, Y. Zang, M. Gu, Y.

Zhang, W. Gao, H. Huyan, W. Guo, D. Wu, Z. Gu, E. Y. Tsymbal, P. Wang, Y. Nie and X. Pan, Nature **570**, 87 (2019).
[19] I. Yamada, Journal of the Physical Society of Japan **33**, 979 (1972).
[20] S. E. McLain, M. R. Dolgos, D. A. Tennant, J. F. Turner, T. Barnes, T. Proffen, B. C. Sales and R. I. Bewley, Nature materials **5**, 561 (2006).
[21] J. Als-Nielsen, S. Bramwell, M. Hutchings, G. McIntyre and D. Visser, Journal of Physics: Condensed Matter **5**, 7871 (1993).
[22] B. Sachs, T. Wehling, K. Novoselov, A. Lichtenstein and M. Katsnelson, Physical Review B **88**, 201402 (2013).
[23] J. Xu, C. Xu, J.-B. Liu, L. Bellaiche, H. Xiang, B.-X. Liu and B. Huang, npj Computational Materials **5**, 1 (2019).
[24] F. İyikanat, E. Sari and H. Sahin, Physical Review B **96**, 155442 (2017).
[25] J. Zhang, X. Shen, Y. Wang, C. Ji, Y. Zhou, J. Wang, F. Huang and X. Lu, Phys. Rev. Lett. **125**, 017601 (2020).
[26] Y. Bai, K. Deng and E. Kan, Physical Chemistry Chemical Physics **18**, 15765 (2016).
[27] J. Goodenough, Annual review of materials science **28**, 1 (1998).
[28] K. I. Kugel and D. Khomskiĭ, Soviet Physics Uspekhi **25**, 231 (1982).
[29] B. Pandey, Y. Zhang, N. Kaushal, R. Soni, L.-F. Lin, W.-J. Hu, G. Alvarez and E. Dagotto, Physical Review B **103**, 045115 (2021).
[30] L.-F. Lin, N. Kaushal, Y. Zhang, A. Moreo and E. Dagotto, Physical Review Materials **5**, 025001 (2021).
[31] S. Ruddlesden and P. Popper, Acta Crystallographica **10**, 538 (1957).
[32] E.-J. Kan, L.-F. Yuan, J. Yang and J. Hou, Physical Review B **76**, 024417 (2007).
[33] F. Aguado, F. Rodríguez, R. Valiente, A. Señas and I. Goncharenko, J. Phys.: Condens. Matter **16**, 1927 (2004).
[34] W. Wang, S. Dai, X. Li, J. Yang, D. J. Srolovitz and Q. Zheng, Nature communications **6**, 1 (2015).
[35] See Supplemental Material at [URL will be inserted by publisher] for (i) determination of the (FM) magnetic ground state by using different U values; (ii) phonon spectra of the tetragonal phase and orthorhombic phase of monolayer RCC; (iii) the band structure of tetragonal phase Rb2CuCl4 and the changes of band gaps with JT transition; (iv) the angular dependence of magnetic anisotropy energy; (v) the Monte Carlo simulation results of critical temperature on the basis of XY model and Heisenberg model.
[36] D. Kasinathan, K. Koepernik, U. Nitzsche and H. Rosner, Physical review letters **99**, 247210 (2007).
[37] Y. Ito and J. Akimitsu, Journal of the Physical Society of Japan **40**, 1333 (1976).
[38] D. Khomskii and K. Kugel, Solid State Communications **13**, 763 (1973).
[39] A. Liechtenstein, V. I. Anisimov and J. Zaanen, Physical Review B **52**, R5467 (1995).
[40] D. Kasinathan, A. Kyker and D. Singh, Physical Review B **73**, 214420 (2006).
[41] H. Witteveen, Physica **71**, 204 (1974).
[42] F. Xue, Y. Hou, Z. Wang and R. Wu, Physical Review B **100**, 224429 (2019).

[43] L. Webster and J.-A. Yan, Physical Review B **98**, 144411 (2018).
[44] S. S. Hong, M. Gu, M. Verma, V. Harbola, B. Y. Wang, D. Lu, A. Vailionis, Y. Hikita, R. Pentcheva and J. M. Rondinelli, Science **368**, 71 (2020).
[45] C. Şen and E. Dagotto, Physical Review B **102**, 035126 (2020).
[46] D. Kozlenko, S. Kichanov, V. I. Voronin, B. Savenko, V. P. Glazkov, E. Kiseleva and N. Proskurnina, J. Exp. Theor. Phys. Lett. **82**, 447 (2005).
[47] N. Terada, C. V. Colin, N. Qureshi, T. C. Hansen, K. Matsubayashi, Y. Uwatoko and A. A. Belik, Phys. Rev. B **102**, 094412 (2020).
[48] T. Terashima, N. Kikugawa, S. Kasahara, T. Watashige, Y. Matsuda, T. Shibauchi and S. Uji, Phys. Rev. B **93**, 180503 (2016).
[49] F. Aguado, F. Rodríguez, R. Valiente, M. Hanfland and J. Itie, Journal of Physics: Condensed Matter **19**, 346229 (2007).
[50] F. Aguado, F. Rodríguez, R. Valiente, J.-P. Itie and M. Hanfland, Physical Review B **85**, 100101 (2012).